TECHNICAL REPORT No. 2310

N84-28058

MULTIPATH INDUCED ERRORS IN METEOROLOGICAL DOPPLER/INTERFEROMETER LOCATION SYSTEMS

FINAL REPORT

APRIL 1984

PREPARED UNDER CONTRACT NAS5-27641, TASK III
FOR GODDARD SPACE FLIGHT CENTER
NATIONAL AERONAUTICS AND SPACE ADMINISTRATION
GREENBELT, MARYLAND 20771

Technical Report Documentation Page

1. Report No.	2. Government Accession No.	3. Recipient's Catalog No.

4. Title and Subtitle

Multipath Induced Errors in Meteorological Doppler/Interferometer Location Systems

5. Report Date
April 1984

6. Performing Organization Code

7. Author(s)
Ronald G. Wallace

8. Performing Organization Report No.
TR 2310

9. Performing Organization Name and Address
ORI, Inc.
1400 Spring Street
Silver Spring, MD 20910

10. Work Unit No. (TRAIS)

11. Contract or Grant No.
NAS5-27641, Task III

12. Sponsoring Agency Name and Address
Instrument Systems Division
NASA/Goddard Space Flight Center
Greenbelt, Maryland 20771

13. Type of Report and Period Covered
Final
March 1984 - April 1984

14. Sponsoring Agency Code
974.0

15. Supplementary Notes

Technical Officer: Jan Turkiewicz

16. Abstract

This report describes one of three study tasks related to the application of an RF interferometer aboard a low-orbiting spacecraft to determine the location of ground-based transmitters. One application of such a system is in tracking high-altitude balloons for meteorological studies. A source of error in this application is reflection of the signal from the sea surface. Through propagation and signal analysis, estimates were made of the magnitude of the reflection-induced error in both Doppler frequency measurements and interferometer phase measurements. The theory of diffuse scattering from random surfaces was applied to obtain the power spectral density of the reflected signal. The processing of the combined direct and reflected signals was then analyzed to find the statistics of the measurement error. It was found that the error varies greatly during the satellite overpass and attains its maximum value at closest approach. The maximum values of interferometer phase error and Doppler frequency error found for the system configuration considered were comparable to thermal noise-induced error.

17. Key Words	18. Distribution Statement
RF Interferometry Wave Propagation Satellite-Based Position Location	

19. Security Classif. (of this report)	20. Security Classif. (of this page)	21. No. of Pages	22. Price
Unclassified	Unclassified	44	

TECHNICAL REPORT No. 2310

ORI
Silver Spring, Maryland 20910

MULTIPATH INDUCED ERRORS IN METEOROLOGICAL DOPPLER/INTERFEROMETER LOCATION SYSTEMS

FINAL REPORT

APRIL 1984

PREPARED UNDER CONTRACT NAS5-27641, TASK III
FOR GODDARD SPACE FLIGHT CENTER
NATIONAL AERONAUTICS AND SPACE ADMININSTRATION
GREENBELT, MARYLAND 20771

TABLE OF CONTENTS

LIST OF FIGURES

I. INTRODUCTION

1.1 SATELLITE-BASED POSITION-LOCATION SYSTEMS

It is possible to determine the location of a ground-based transmitter by observing the Doppler variation of the signal frequency as received aboard a low-orbiting satellite as it passes within view of the transmitter. This technique is employed by ARGOS, a data collection and location service jointly operated by CNES (Center National d'Etudes Spatiales) in France, and NOAA and NASA in the U.S. The ARGOS flight instruments, carried by the TIROS series of meteorological satellites, record frequency measurement and digitally encoded environmental data from worldwide data collection platforms (typically buoys and balloons), and relay this information to the ground, where it is processed to extract the platform positions, and provided to the platform owners. The experimental SARSAT (Search and Rescue Satellite-Aided Tracking) System, which is also carried on TIROS, uses Doppler position location as well.

RF interferometry is another technique for position location from spacecraft. While the received signal frequency is used in the Doppler technique, the received signal phase difference, observed between two antennas, is used by an interferometer to locate the transmitter. The antennas are attached to the spacecraft on either end of a baseline of accurately known length and orientation. In practice, an interferometer requires more than two antennas so that location ambiguities, inherent to the technique, can be resolved. The RF interferometer method has not yet been

applied to position location from satellites, although an interferometer was flown aboard the ATS-6 spacecraft for precision attitude determination. Studies have shown that applying the interferometer and Doppler techniques in combination can yield significant improvements in location performance over that of a Doppler-only system (Reed and Wallace - 1981.).

1.2 METEOROLOGICAL APPLICATIONS AND THE MULTIPATH PROBLEM

An important application of space-based position location systems is tracking high-altitude balloons to map global wind patterns. The Tropical Winds Energy Reference Level Experiment (TWERLE) employed the RAMS (Random Access Measurement System) aboard NIMBUS-6 to accomplish this. The RAMS used the Doppler technique of position location. An improved position location system has been proposed for this application that uses an RF Interferometer in addition to Doppler processing (Wallace and Reed - 1981). It would employ an interferometer having a relatively long baseline to make high-resolution measurements of balloon velocity, as well as location. This system would determine velocity averaged over a period on the order of ten minutes, rather than over the period of a spacecraft orbit (100 minutes), which is required using Doppler alone.

A source of location error that may be especially significant in the application of an RF interferometer to locating high-altitude platforms is multipath reflection from the sea surface. The magnitude of this multipath-induced error in interferometers and Doppler processing instruments was the subject of the study reported herein. It was found (see Section IV) that the error with an interferometer can be at most twice that induced by thermal noise in the receiver, and that the error at any instant during the satellite overpass is highly dependent on the position of the satellite relative to the platform. Errors in Doppler systems due to multipath were found to be comparable to thermal noise error. In addition, it was found that the errors can be minimized by using circular polarization on the RF link, a platform antenna pattern that discriminates against reflections, and narrowband filtering in the receiver. Another significant conclusion is that the multipath induces no bias in the position measurement of either interferometer or Doppler instruments.

1.3 DESCRIPTION OF SYSTEM ANALYZED

The multipath error analysis was based on a spaceborne interferometer position location system having parameters listed in Table 1.1. In what follows, we give a general description of the system, and justification and elaboration of the parameters.

The system consists of a flight instrument, flown aboard a low-orbiting satellite, the data collection platforms, and a ground processing system. The satellite is in a sun-synchronous orbit, providing full global coverage every 12 hours. The flight instrument includes two identical wide-beam antennas, with patterns that are symmetrical about nadir. The antennas are mounted to the spacecraft on a baseline oriented perpendicular to the satellite's velocity vector. The instrument measures the frequency of the received platform signals with respect to a stable internal reference, and the phase difference between the two antennas. The noise accompanying the signal is reduced with a narrowband filter prior to making the phase and frequency measurements. To further reduce noise-induced error, the measurements are averaged over an interval of about a third of a second.

The data collection platforms are assumed to be drifting high-altitude balloons that carry sensors, batteries, and transmitters. Each transmitter sends a short UHF burst approximately once per minute. The burst duration is at least sufficient to allow the spacecraft to make required averaged phase and frequency measurements. Part of the burst is digitally modulated with platform identification and sensor data. The platform antenna pattern is symmetrical about the vertical, ideally having low gain below the horizontal. The effect of the platform antenna pattern on the multipath error is considered later.

Through onboard recording and playback, or direct relay, the ground processor receives the phase and frequency measurements and digital data obtained from the platforms. By combining satellite ephemeris and attitude with the measurements, the processor computes the estimated location of the platforms.

TABLE 1.1

SYSTEM PARAMETERS

Satellite Orbit	Sun Synchronous, 830 km Altitude
Interferometer Antenna Baseline Length	20 m
Interferometer Antenna Baseline Orientation	Perpendicular to Satellite Velocity Vector
Platform Height	20 km
Platform Location	Randomly, Over Ocean
Platform Burst Frequency	401 MHz
Platform Burst Length	Greater than 300 ms
Received Carrier-to-Noise Density Ratio	40 dB-Hz minimum
Measurement Filter Bandwidth	30 Hz
Measurement Averaging Time	300 ms

1.4 PREVIOUS RESULTS

The effects of multipath reflections from the earth's surface on satellite-based position location and communications systems have been examined previously (Durrani and Staras - 1968, Meuhldorf - 1971, Staras - 1968, Duncan - 1967). Durrani and Staras considered the situation of a geostationary relay satellite (e.g., TDRS) receiving a signal from a low-orbiting satellite. Their concern was the decrease in carrier-to-noise ratio, and resulting increase in bit error rate, caused by multipath reflections from the surface. Muehldorf considered a problem more similar to the present one - a geostationary interferometer for position location. He estimated the location error due to multipath reflections and found it, with adequate measurement filtering, to be negligible.

The two previously studied problems and the present one all consider the simultaneous reception of two signals, one direct and one indirect off the earth's surface. The differences are geometric and dynamic. The altitude of the receiver in the previous cases is nearly fifty times that of the present case. The transmitter in Mueldorf's case was assumed to be in an aircraft, having an altitude of 10-30 km, and a velocity of 300 to 1000 km/hr. In Staras and Durrani's case, the transmitter was in a low-orbiting satellite, at 160-640 km altitude and moving at approximately 8 km/sec. The approach used in the previous two studies cited was the same, and it is the approach chosen in the present case. The results in all three cases are, not surprisingly, qualitatively similar, but the geometric and dynamic differences lead to quite different quantitative solutions.

1.5 QUALITATIVE RESULTS

Before delving into the mathematics, we shall describe the nature of the mechanisms leading to multipath location errors and present a qualitative picture of how they behave.

Assume for the moment that the earth's surface was perfectly smooth, and that the transmitter and receiver were somehow suspended motionless over the surface within mutual visibility. From the viewpoint of the receiver, there would appear to be two transmitters: the actual one, and an image beneath the surface. The image would be located in the plane containing the actual transmitter, the receiver, and the center of the earth; and would appear to be under the surface a distance slightly less than the actual transmitter's height over the surface. The amplitude of the signal from the image is something less than that from the transmitter, due to its greater (apparent) distance from the receiver, and a less-than-unity reflection coefficient at the surface. The phase of the image signal is retarded by many wavelengths with respect to the direct signal because of the greater distance the reflected signal must travel.

The effect of this image signal on an interferometer can be seen by examining Figure 1.1. In the upper part of the figure, vectors D_1 and D_2 represent the direct signal received at the two interferometer antennas.

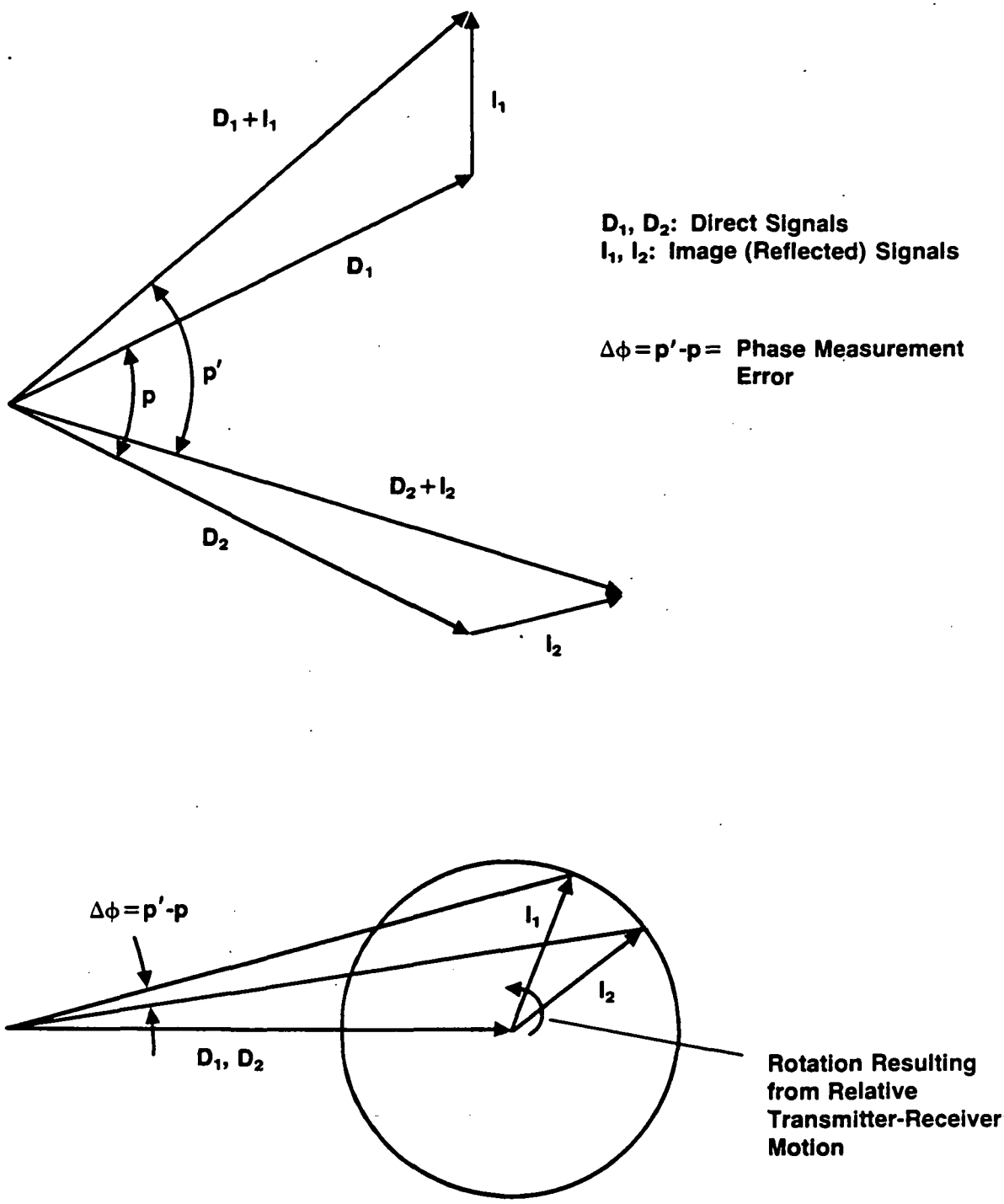

FIGURE 1.1. SIGNAL VECTOR ANALYSIS

Their electrical phase difference P is related to the space angle between the antenna baseline direction and the direction of signal arrival. The vectors I_1 and I_2 represent the image signals received at the two antennas. The total signal received at each antenna is the vector sum of the direct and image signals. The angle between the direct and image signals at each antenna is determined by the difference in their path lengths. The angle between I_1 and I_2 is a function of the direction of arrival of the image signal, and is in general different from P because the image and actual transmitter signals arrive from different directions. The apparent phase difference seen by the interferometer, with the image present, is P' as shown. The error in the measured phase angle introduced by the reflection, $\Delta\phi = P'-P$, is the quantity of interest. The vector diagram can be modified to show $\Delta\phi$ more clearly by making P = 0. This results in D_1 and D_2 coinciding and the tails of I_1 and I_2 being joined as shown in the lower part of the figure.

Now assume that there is relative motion between the transmitter and receiver. As the distance between the transmitter and receiver changes due to this motion, the distance between the image transmitter and the receiver also changes, but at a different rate. Over a short interval, the receiver-to-actual transmitter range changes by, say, δR meters, while the receiver-to-image transmitter range changes by $\delta R'$. The difference between δR and $\delta R'$ is seen at the interferometer as a change in phase between the direct and image signals. If we assume further that the directions of arrival of the direct and image signals changes very little over this interval, the phase change is the same at both interferometer antennas. The result of the motion is therefore a rotation of the pair of vectors, I_1 and I_2, with very little change in the angle between them. The rotation is indicated in the lower part of the figure. The rate of this rotation is equal to the difference in the Doppler frequency shift between the actual and image transmitters. As the vectors rotate, the phase error $\Delta\phi$ oscillates about zero as shown in Figure 1.2. As one might guess from the shape of the waveform, the average value of $\Delta\phi$ is found to be zero.

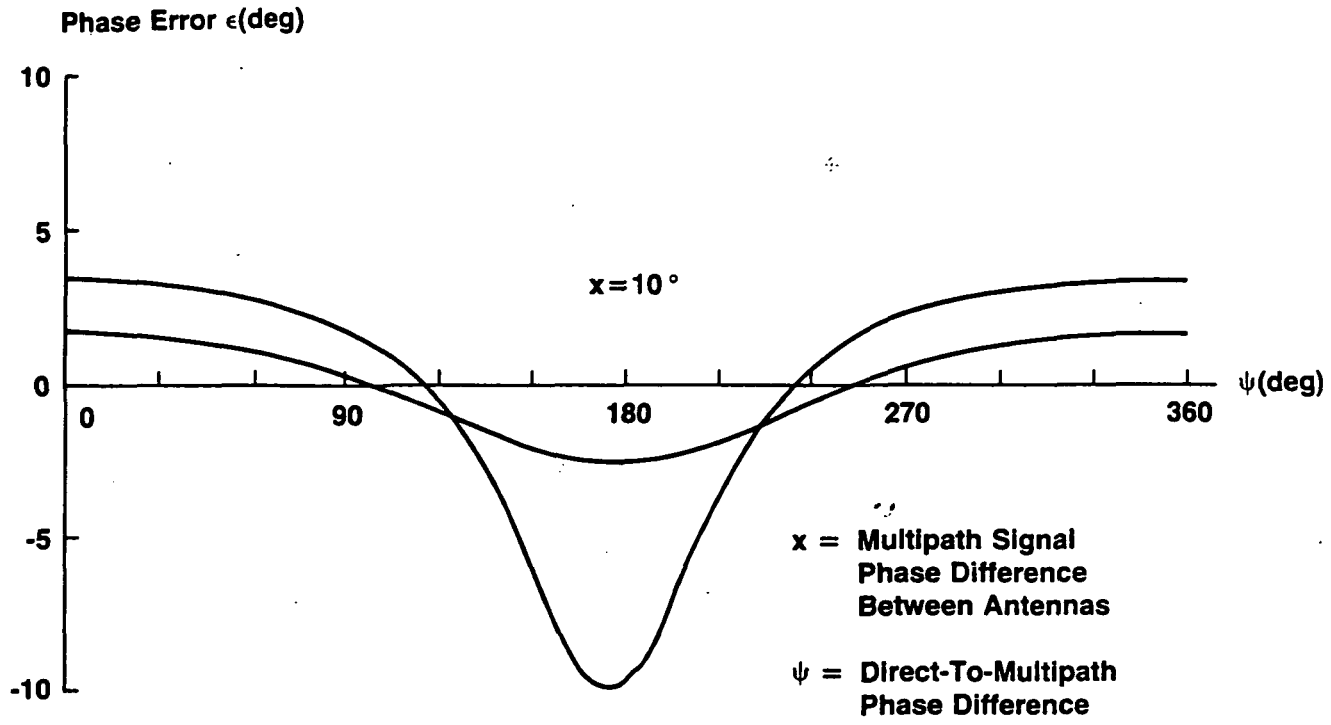

FIGURE 1.2. PHASE ANGLE MEASUREMENT ERROR

We now drop the stipulation that the earth's surface is smooth and allow for the effects of ocean waves on the multipath error. the smooth surface assumption used earlier is applicable to some degree when the sea surface reflections occur at very low incidence angles. In that case, the reflection is specular. Of more interest in our current problem are diffuse reflections, which occur at higher angles of incidence. With diffuse reflection, the concept of an image loses its meaning, because reflections do not appear to come from a localized point source. Rather, the reflections come from a smear or patch on the surface without sharply defined boundaries. The patch is elliptically-shaped, and its center is the point where a line between the receiver and an image transmitter (if the surface were smooth and there were one) would pierce the surface. This will be called the "specular reflection point." Its location is easily determined by geometric optics. The reflected signal received from this patch is constantly varying in amplitude and phase. It can be characterized by its average power (or mean square amplitude) and its power spectral density.

The power spectral density of the reflected signal turns out to have a Gaussian shape that is centered at the Doppler frequency corresponding to the rate of change of the range between the receiver and the image transmitter (again, if there were one). Because the receiver-to-actual transmitter range rate and the receiver-to-image transmitter range rate differ, there will in general be a frequency offset between the direct received signal and the center of the received reflected signal spectrum. This offset disappears when the range rate difference goes through zero, which occurs at the point of closest approach.

This behavior is illustrated in Figure 1.3, which shows the received signal spectrum at selected instants during two satellite overpasses in the vicinity of an elevated transmitter. Note that the center of the reflected signal spectrum is below the direct signal's frequency when the satellite is approaching the transmitter, and the opposite is so when the satellite is departing. At closest approach (the two middle satellite locations in the figure), the reflected signal's spectrum center coincides with the direct signal. The frequency spreading of the reflected signal power, at least for the geometry of interest here, is due mainly to the distribution of relative velocities, and therefore of Doppler shifts, over the reflecting patch. The received reflected signal is actually the sum of innumerable components coming from the sea surface "facets" that happen to be oriented properly at any given instant. The reflection from each facet is Doppler shifted by an amount determined by the location of the facet in the patch, through the geometrical variables applying to that location. The distribution of reflecting facets over the patch therefore results in a distribution of frequencies in the composite reflected signal. The extent of the facet distribution changes with the overpass geometry, and so does the width of the reflected signal spectrum. As shown in Figure 1.3, the width of the spectrum is greater for a near-overhead pass than it is for a pass with an appreciable closest-approach distance from the transmitter.

We now consider the effect of the diffuse multipath reflections on interferometer location measurements. The interferometer on the satellite

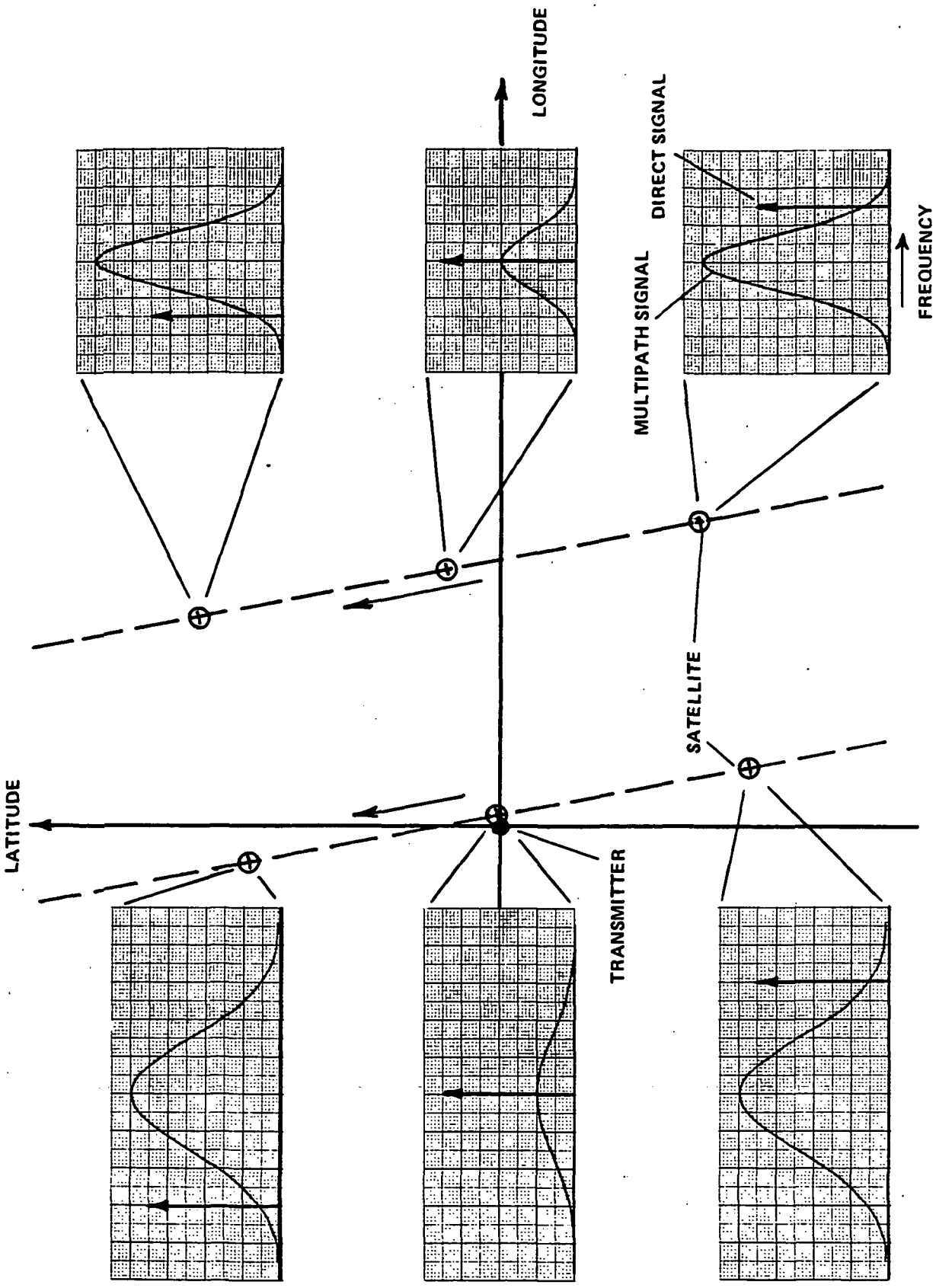

FIGURE 1.3. RECEIVED SIGNAL SPECTRA FOR VARIOUS SATELLITE LOCATIONS

contains a phase-lock loop that tracks and narrowly filters the direct signal. The phase measurement error due to multipath varies directly with the amount of reflected signal power that falls within the filter passband, which is centered on the direct signal. The reflected power in the filter passband depends on the total power reflected, the width of the reflected signal spectrum, and the offset of the reflected signal spectrum from the direct signal. These three factors vary simultaneously with satellite position, so one would expect the error to vary in a complex way during an overpass.

It is possible to reduce the multipath error by using circular polarization. This is because waves reflected from the surface of water undergo a change of rotation sense. Right-hand circularly polarized waves, for example, are reflected from the surface as left-hand circularly polarized waves due to the Fresnel reflection coefficient's angle being near 180^{o}. Using a receiving antenna that is sensitive to only the sense of circular polarization that is transmitted provides a means of rejecting most of the reflected power. This rejection is total when the incidence angle is 90^{o} (transmitter directly below receiver), and becomes less as the incidence angle decreases. Figure 1.3 shows this effect. The amplitude of the reflected signal spectrum is minimum at the point of closest approach for both overpasses. The minimum is smaller for the close (left-hand) pass than it is for the pass further from the transmitter.

The remainder of this report is a detailed analysis of the factors discussed above, arriving at numerical results for the system hypothesized.

II. ERROR ANALYSIS

2.1 PHASE MEASUREMENT ERROR

Figure 2.1 shows the basic geometry of an interferometer. The plane of the figures is that defined by the interferometer antennas and the transmitter. Two signals are received: the direct signal at angle with respect to the bisector of the antenna baseline, and the reflected signal. The reflected signal source is the image, which is not, in general, in the plane of the figure. The angle of arrival of the reflected signal, ', is therefore measured in the plane defined by the antennas and image. The direct and image signals (D and I, respectively) received by the two antennas (labelled 1 and 2) are described in phasor notation as follows:

Direct Signal:	$D_1 = 1 \angle 0$
	$D_2 = 1 \angle p$
Image Signal:	$I_1 = \rho \angle \chi$
	$I_2 = \rho \angle \chi + x$

These phasors are shown in Figure 2.2. The phase difference p is related to the direct signal's angle of arrival η by

$$p = (2\pi L/\lambda) \sin$$

Likewise, the phase difference x is related to the angle of arrival of the reflected signal, η', by

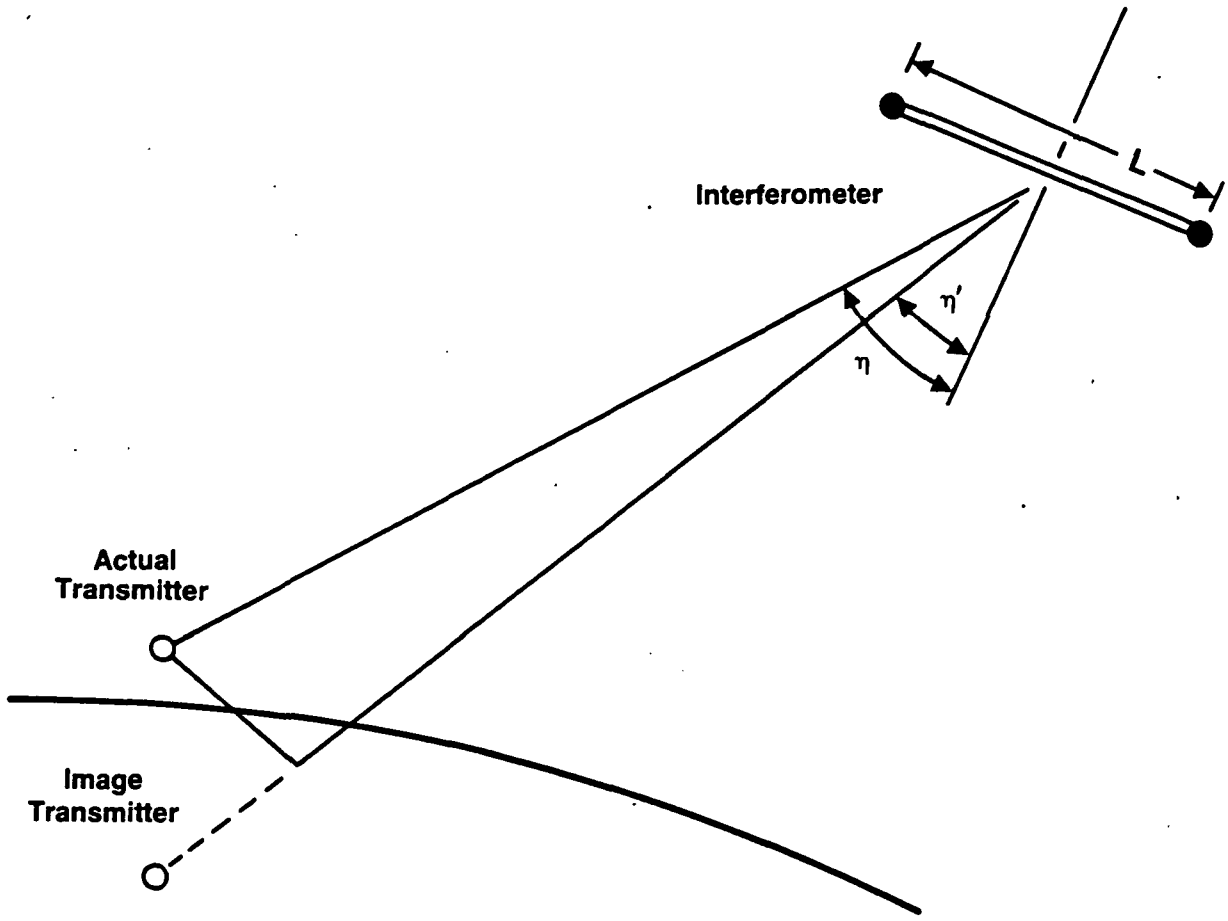

FIGURE 2.1 INTERFEROMETER GEOMETRY

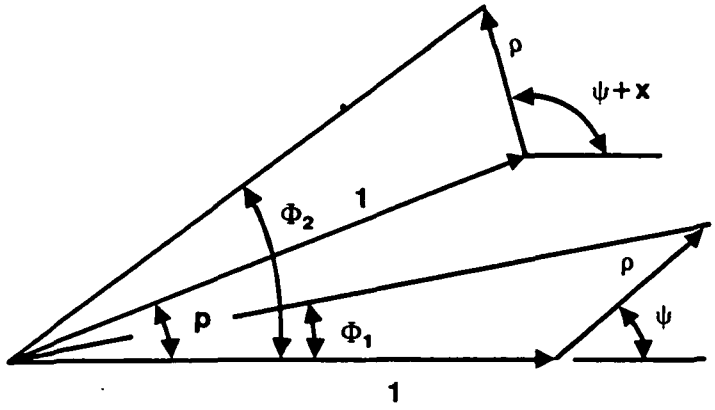

FIGURE 2.2. PHASOR DEFINITIONS

$$x = (2\pi L/\lambda) \sin \eta'$$

The angle x is that corresponding to the difference between the range to the actual transmitter and that to the image (plus any additional phase lag introduced by the surface reflection), modulo 2π.

Introducing the angle $\epsilon = \eta - \eta'$ which is small ($< 2^0$) for the geometry considered, we can make the approximation

$$x \cong (2\pi L/\lambda) \cos$$

The phase angles of the resultant phasors at antennas 1 and 2 are found to be

$$\Phi_1 = Arg(D_1 + I_1) = \tan^{-1}\left[\frac{\rho \cos\Psi}{1+\rho\cos\Psi}\right]$$

$$\Phi_2 = Arg(D_2 + I_2) = p + \tan^{-1}\left[\frac{\rho \sin(\Psi+x)}{1+\rho\cos(\Psi+x)}\right]$$

Without the reflection present ($\rho = 0$), the phase difference $\Phi_2 - \Phi_1$, is p, as expected. The error in phase measurement introduced by the reflection is then $\Phi_2 - \Phi_1$, minus p, or

$$\Delta\phi = \tan^{-1}\left[\frac{\rho \sin(\Psi+x)}{1+\rho\cos(\Psi+x)}\right] - \tan^{-1}\left[\frac{\rho \sin\Psi}{1+\rho\cos\Psi}\right]$$

As long as $\rho < 0.3$, the phase measurement error is well-approximated by (Mueldorf)

$$\Delta\phi \cong 2\rho \sin(x/2) \cos(\Psi + x/2)$$

The reflected signal is the sum of a large number of random vectors, each corresponding to the reflection from a facet of the rough surface. It is well known that the amplitude of such a signal may be characterized as Rayleigh, having the following probability density function

$$f_\rho(r) = (r/\sigma^2) \exp(-r^2/2\sigma^2)$$

The parameter σ^2 is one-half the mean square value of ρ, or $\overline{\rho^2}/2$. Furthermore, the phase of the reflected signal is uniformly distributed:

$$f_\psi(\psi) = 1/2\pi \qquad 0 \le \psi \le 2\pi$$
$$= 0 \qquad \text{otherwise}$$

These density functions will now be applied to find the mean and variance of the phase measurement error. Clearly the mean must be zero. Using the approximation, we calculate the expectation over ψ:

$$E(\Delta\phi) = 2\rho \sin(x/2) \int_0^{2\pi} \cos(\psi + x/2)\, d\psi = 0$$

Alternately, it may be noted that each term of the exact expressions for $\Delta\phi$ individually integrates to zero.

The variance of the phase error, which is also the variance of the measured phase, $\text{Var}(\phi) = \sigma_\phi^2$, is found by performing the following integration (again, using the approximation):

$$\sigma_\phi^2 = \frac{1}{2\pi} \int_0^{2\pi} \int_0^{\infty} \left[2r \sin(x/2) \cos(\psi + x/2)\right]^2 f_\rho(r)\, d\psi\, dr$$
$$= 2\overline{\rho^2} \sin^2(x/2) = \left[2\sigma^2 \sin(x/2)\right]^2$$

By numerically performing the integration of the exact expression, it was found that this approximation can be improved for $\rho \le 0.3$ by increasing it by 5 percent.

An actual phase measuring instrument used in an interferometer would reduce random errors by averaging the measurement over an integration period. The effectiveness of this averaging in reducing noise-induced errors depends on the duration of the integration period compared with the reciprocal of the measurement filter bandwidth, B. It can be shown (Reed and Wallace - 1981) that when the integration period T is greater than about four times the reciprocal bandwidth, or $T > 4/B$, then the variance of the random noise error is reduced by a factor of $(BT)^{-1}$. This is strictly true only when the noise

has a flat spectrum, but it is a good approximation in the present case if the filter bandwidth is sufficiently narrow.

Including the averaging effect (and the 5 percent approximation improvement) in the phase error variance expression, we have

$$\sigma_\phi^2 \cong 2.1\,(BT)^{-1}\,\overline{\rho^2}\,\sin^2(x/2)$$

2.2 FREQUENCY MEASUREMENT ERROR

The multipath-induced error in the measurement of frequency is dependent on the phase variance and the integration time. Blanchard (1976) shows that when the integration time is long enough so that the phase noise at the beginning and end of the period can be considered independent, then the variance of the measured frequency, σ_f^2, is given by

$$\sigma_f^2 = \sigma_\theta^2 / (2\pi^2 T^2)$$

where σ_θ^2 is the variance of the signal phase (in square radians). The signal phase in this case is different from the phase difference, p, that the interferometer measures because only the output of one antenna is used to measure frequency. Using the previous phasor notation, we have for the phase of the signal received at antenna 1:

$$\theta = \text{Arg}\,(D_1 + I_1) = \text{Arg}\,(1\angle 0 + \rho\angle\psi)$$

$$= \tan^{-1}\left[\frac{\rho\sin\psi}{1+\rho\cos\psi}\right]$$

For $\rho < 0.3$, the following approximation is acceptable

$$\theta \cong \rho\sin\psi$$

Using the previously stated statistics of ρ and ψ, we find

$$E(\theta) = 0$$

$$E(\theta^2) = \sigma_\theta^2 = \overline{\rho^2}/2$$

Substituting this into the expression for the frequency gives

$$\sigma_f^2 = \overline{\rho^2}/(2\pi T)^2$$

III. CHARACTERIZING THE REFLECTED SIGNAL

The objective of this section is to arrive at expressions for $\overline{\rho^2}$, the mean square reflected signal relative to the direct signal that is seen at the output of the measurement filter. We begin by introducing a model that describes diffuse reflections from the sea surface. The model is applied to the particular geometry of interest, and the reflected signal power spectral density is calculated. This power spectral density is then scaled by a reflection discrimination factor that results from using circular polarization. Finally, the frequency and phase measurement errors are calculated as functions of receiver location with respect to the transmitter.

3.1 SEA SURFACE REFLECTIONS

When electromagnetic waves are incident upon any rough surface, such as the sea surface, two types of reflection can occur: specular reflection and diffuse scattering. They can both be present simultaneously, and the one that predominates is determined by the "roughness" of the surface as seen by the incoming wave. A commonly used "roughness" criterion is the Rayleigh criterion:

$$\sigma_h \underset{\text{diff}}{\overset{\text{spec}}{\lessgtr}} \frac{\lambda}{8 \sin\theta}$$

where σ_h is the standard deviation of the height of the surface, λ is the electrical wavelength, and θ is the angle of arrival of the incident wave with respect to the horizontal or the grazing angle. This says that increasing the

wavelength, decreasing the standard deviation of the surface height, and decreasing the grazing angle all result in a large specular component of the reflected field. To show what type of reflection predominates in our problem, Table 3.1 gives the grazing angle just satisfying the Rayleigh criterion for various sea states at 400 MHz. Also given are the values of σ_h assumed to correspond to each sea state (based on the World Meteorological Organization definition).

TABLE 3.1

GRAZING ANGLES FOR SPECULAR REFLECTION AT 400 MHz

Sea State	Standard Deviation of Wave Height	Maximum Grazing Angle for Specular Reflection
1	.05 m	-
2	.3	18.2^0
3	.9	5.0^0
4	1.8	3.0^0
5	3.2	1.7^0
6	5.0	1.1^0
7	7.5	0.7^0

According to the table, the sea must be fairly calm (sea state 3 or less) for there to be much specular reflection above a 10^0 grazing angle. We shall concentrate on the diffuse component of reflection in this analysis because the elevation angle of the satellite is expected to be at least 10^0. It should be borne in mind, however, that the applicability of the results obtained may be suspect for calm seas and low grazing angles.

The surface producing diffuse scattering requires a second parameter, besides , to describe it statistically. That parameter is T, the correlation distance along the surface. This is the distance over which the correlation function of the height drops to 1/e or 0.37. A third important parameter of the surface, which is derived from the first two, is β_0:

$$\beta_0 = \tan^{-1} (2\sigma_h/T)$$

Because σ_h and T are characteristic vertical and horizontal dimensions of the surface, β_0 can be thought of as a kind of average absolute slope.

According to the model developed by Beckmann and Spizzichino (1963), the mean power received at the satellite, $\overline{dP}$, due to reflection by an arbitrary element of the surface of area dS, is given by

$$\overline{dP} \approx P_d \, dS \frac{D r^2}{4\pi r_1^2 r_2^2} \frac{\cot^2\beta_0}{\cos^4\beta} \exp\left[-\frac{\tan^2\beta}{\tan^2\beta_0}\right]$$

where P_d is the power received directly from the transmitter and the geometric variables are defined in Figure 3.1. D is the divergence factor, accounting for the curvature of the surface. The angle β is that between the local vertical at dS and the bisector of the rays r_1 and r_2. This equation assumes isotropic antennas on both the transmitter and receiver, and a perfectly conducting earth. (The actual surface reflection coefficient will be incorporated later.) The approximation also assumes that the radius of curvature of the surface irregularities is large compared with a wavelength and that $\sigma_h^2 >> (\lambda/2\pi)^2$. Note from the expression that dP is maximum at the point of specular reflection, where $\beta = 0$. The value of tan $_0$ is usually taken to be on the order of 0.1, so $\overline{dP}$ falls off quickly as dS is moved away from the specular reflection point. The variation of β over the surface is shown in Figure 3.2 for a satellite/transmitter separation angle of 10^0.

The total power received can be found by integrating $\overline{dP}$ as dS is moved over the surface. This will not be done directly. Instead we shall introduce dynamics by assuming a moving receiver, then compute the autocorrelation function of the received signal. The autocorrelation function then shall be used to find the power spectral density, which will give the frequency offset, the spectrum width, and eventually the average reflected power obtained at the output of the measurement filter, $\overline{\rho^2}$.

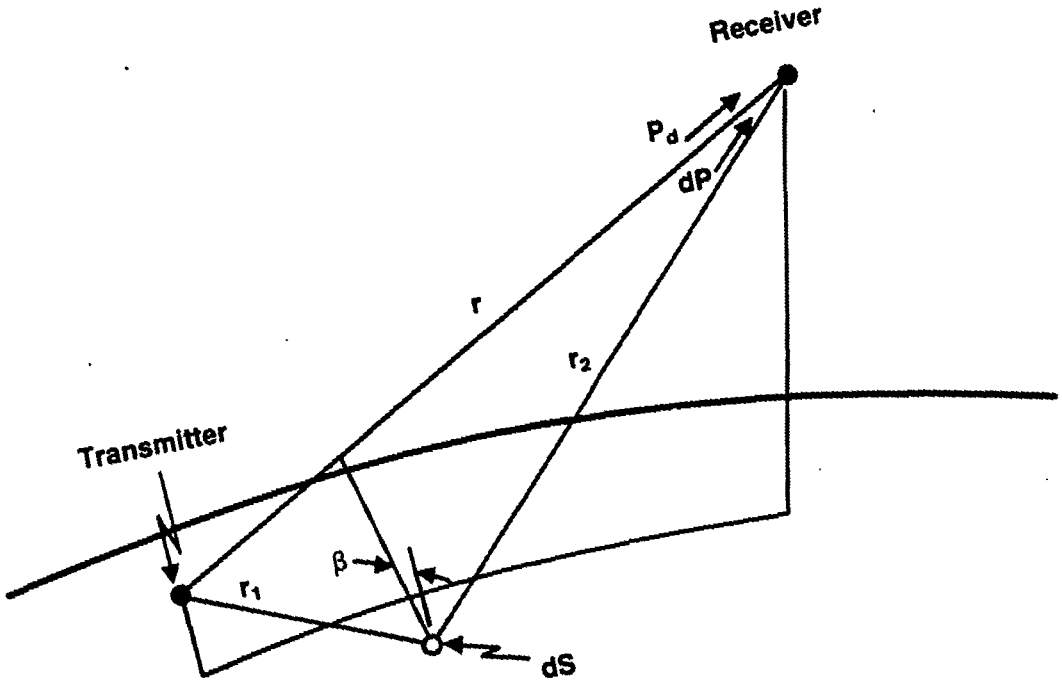

FIGURE 3.1. DEFINITION OF GEOMETRIC VARIABLES

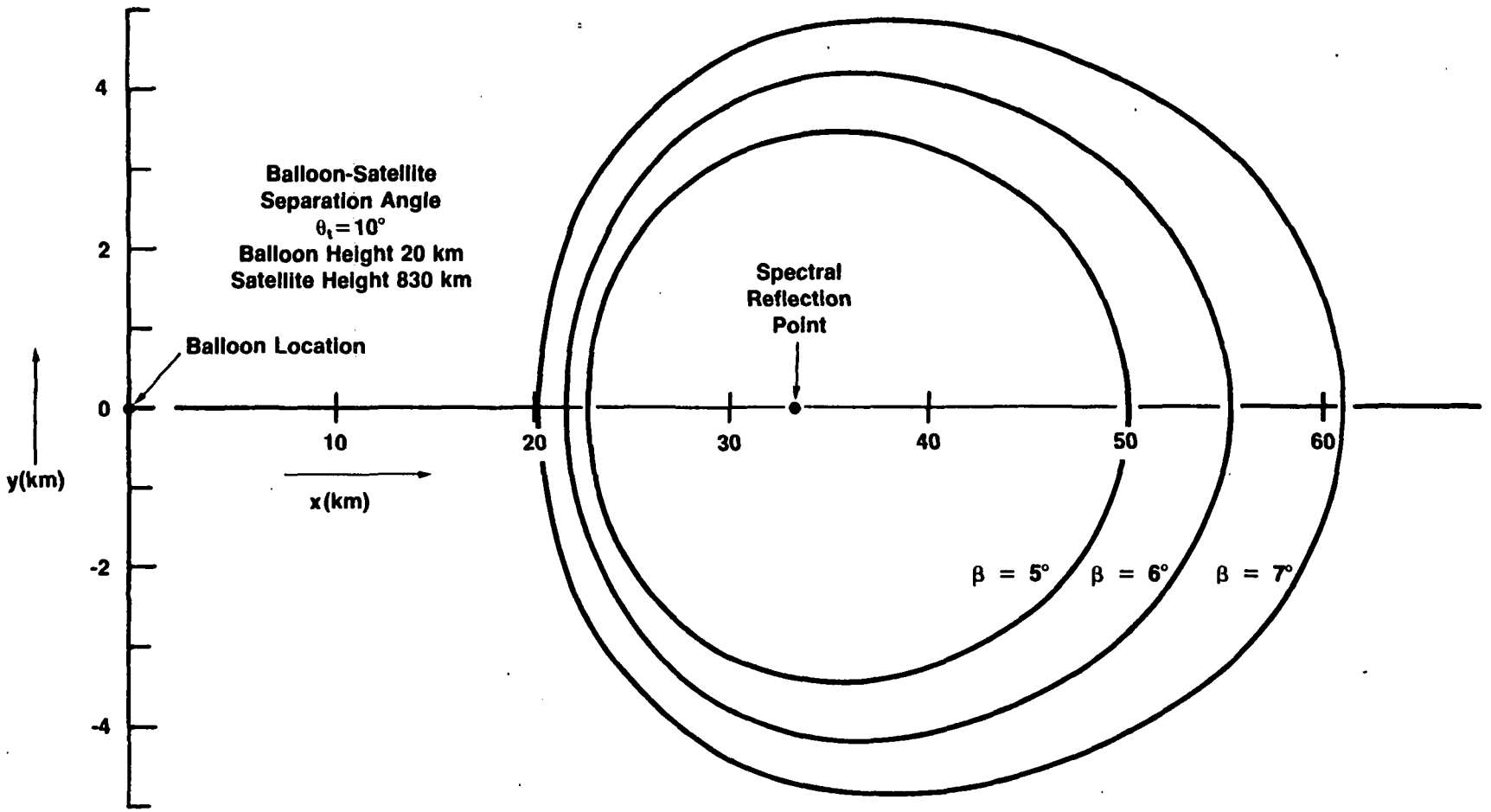

FIGURE 3.2. CONTOURS FOR ANGLE β BETWEEN LOCAL VERTICAL AND BISECTOR OF RAYS

3.2 DETERMINATION OF REFLECTED POWER SPECTRAL DENSITY

The variables used in the subsequent development are defined in Figure 3.3. The transmitter, receiver, and specular reflection point form a plane, which also includes the center of the earth. The angles θ_s, θ, and θ_t are measured in this plane. The vector $\underline{v}$ is the receiver velocity. This vector is perpendicular to the local vertical and at an angle ϕ_v with respect to the transmitter/receiver/earth center plane.

The autocorrelation function of the received reflected signal e(t) is defined by

$$R_e(\tau) = E\left[e(t)e^*(t+\tau)\right]$$

where e(t) is taken to be a phasor with amplitude and phase varying slowly compared to the RF period. e(t) is actually the sum of a large number of independent phasors, $e_i \angle \phi_i$:

$$e(t) = \sum_i e_i(t) \exp\left[j\phi_i(t) + j\omega_c t\right]$$

We assume that τ is short enough that the magnitude of the phasors does not change between t and $t+\tau$, and that the only phase change is that due to the change in receiver position. This gives

$$e(t+\tau) = \sum_i e_i(t) \exp\left\{j\left[\phi_i(t) - \Delta\phi_i(\tau) + \omega_c(t+\tau)\right]\right\}$$

where $\Delta\phi_i(\tau)$ is a systematic phase change, depending on the location of the reflecting facet of the surface that is responsible for the i^{th} component of the received signal. Since all the components are independent, we can write, from the definition of the autocorrelation function,

$$R_e(\tau) = E\left\{\sum_i e_i(t)e_i^*(t)\exp\left[j\Delta\phi_i(\tau) - j\omega_c\tau\right]\right\}$$

$$= \sum_i E\left[e_i(t)e_i^*(t)\right]\exp\left[j\Delta\phi_i(\tau) - j\omega_c\tau\right]$$

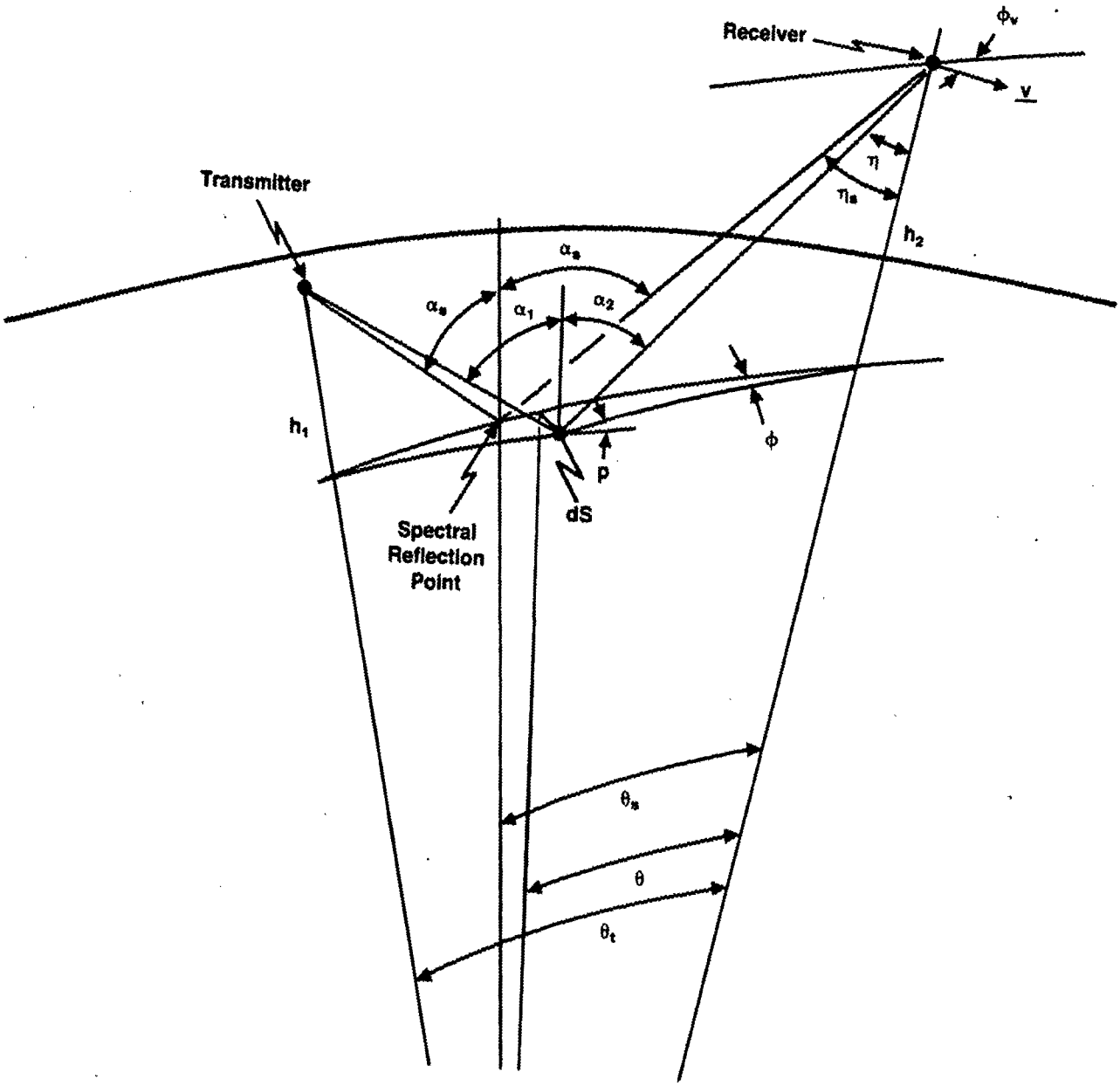

FIGURE 3.3. FURTHER DEFINITION OF VARIABLES

The exponential may be removed from the expectation because the $\Delta\phi_i(\tau)$ are not random. We observe that the term $E\left[e_i(t)e_i^*(t)\right]$ is just the average power of the i^{th} component of the signal. If we assume each component originates at a small area of the surface dS, this term can be replaced by $\overline{dP}(\underline{r}_i)$, where $\underline{r}_i$ denotes the location of dS. At the same time, the phase $\Delta\phi_i(\tau)$ can be replaced by $\Delta\phi(\tau,\underline{r}_i)$. Now, letting the number of components increase without bound, while the surface elements become infinitesimal, the summation becomes an integral over the surface

$$R_e(\tau) = \int_{surface} \exp\left[j\Delta\phi(\tau,\underline{r}) - j\omega_c\tau\right] \overline{p_o}(\underline{r})\, dS$$

where $\overline{p_0}(\underline{r})$ is a power density defined by

$$\overline{dP}(\underline{r}) = \overline{p_0}(\underline{r})\, dS$$

and both the phase and the power density are continuous functions of location on the surface.

The first step in evaluating the integral is to express $\Delta\phi$, β, r_1 and r_2 in terms of the coordinates of points on the surface, $\underline{r} = (\theta,\phi)$. In developing these expressions, approximations allowed by the assumed geometry are used where appropriate. From Figure 3.1, we have

$$\Delta\phi(\tau,\underline{r}) = k\left[\Delta r_1(\tau,\underline{r}) + \Delta r_2(\tau,\underline{r})\right]$$

where $k = 2\pi/\lambda$ and Δr_1 and Δr_2 are the changes in r_1 and r_2 during the short interval τ. We have assumed that the velocity of the transmitter with respect to the surface is negligible compared with the velocity of the receiver, so Δr_1 can be ignored compared with Δr_2. Thus,

$$\Delta\phi(\tau,\underline{r}) \cong k\,\Delta r_2(\tau,\underline{r}) = kv\tau\cos(\phi_v+\phi)\sin\eta$$

where η is the angle to the surface point with respect to nadir at the receiver location.

In the expression for $\overline{dP}$ (or $\overline{p}_0$), the following approximations can be made

$$D \cong 1$$
$$r_2 \cong r$$
$$\cos\beta \cong 1$$

This is permissible because the only significant contribution to the integral occurs for the surface point in the vicinity of the specular reflection point, and for the geometry assumed, the approximations hold near that point. The integral now becomes

$$R_e(\tau) \cong P_d \frac{\cot^2\beta}{4\pi} \int \frac{1}{r_1^2} \exp\left[-\frac{\tan^2\beta}{\tan^2\beta_0} + jkv\cos(\phi_v+\phi)\sin\eta - j\omega_c\tau\right] dS$$

Following the lead of Staras (1968), we shall use the method of steepest descent to approximate the value of the integral. This method uses the fact that the only significant contribution to the integral is near the point where the real part of the exponent is zero, which happens to be the specular reflection point. The exponent is replaced by one or two terms of a Taylor series expansion about that point, and any non-exponential terms of the integral ($1/r_1^2$ in this case) are evaluated at that point and placed before the integral sign. The remaining exponential integrals are then evaluated by expanding the limits of integration to infinity.

The differential element of area dS is given by

$$dS = a^2 \sin\theta \, d\theta \, d\phi$$

where a = earth's radius.

We need a Taylor series expansion for the exponent that holds in the vicinity of the specular reflection point: $\theta = \theta_s$, $\phi = 0$. The first non-zero terms of the expansion of $\tan^2\beta$ are the quadratic terms, as follows

$$\tan^2\beta \cong \frac{1}{4s^2}(\tan^2\alpha_s)\,\phi^2 + M^2(\theta-\theta_s)^2$$

where

$$s = \frac{\sin(\theta_t-\theta_s)}{\sin\theta_t}$$

$$b = h_1/a.$$

The details of the derivation of this and an expression for M are given in the Appendix. The Taylor series expansion of the imaginary exponent in the integral gives a constant and linear terms, in particular,

$$\cos(\phi_v+\phi)\sin\eta \cong \cos\phi_v\sin\eta_s + (N\cos\phi_v)(\theta-\theta_s) - (\sin\phi_v\sin\eta_s)\phi$$

where

$$\eta_s = \alpha_s - \theta_s$$

$$c = h_2/a$$

The Appendix contains the derivation of this and an expression for N. When the exponent is expanded as indicated, and r_1 and θ are evaluated at the specular reflection point, the expression becomes

$$R_e(\tau) \cong (P_d/4\pi)\frac{\sin\theta_s\cot^2\beta_0}{s[b^2+4(1+b)\sin^2(\theta_s/2)]}\exp\left[j\nu\tau\cos\phi_v\sin\eta_s - j\omega_c\tau\right]$$

$$\cdot\int\exp\left[-\frac{\tan^2\alpha_s}{4s^2\tan^2\beta_0}\phi^2 + j\nu\tau\phi\sin\phi_v\sin\eta_s\right]d\phi$$

$$\cdot\int\exp\left[-\frac{M^2}{\tan^2\beta_0}(\theta-\theta_s)^2 - j\nu\tau(\theta-\theta_s)N\cos\phi_v\right]d\theta$$

The limits of integration are only over the reflecting patch, but they can be expanded to infinity with negligible error, owing to the nature of the integrands. Doing this, one finally obtains

$$R_e(\tau) \cong P_d\,Q\exp\left(-\tau^2B^2/2 + j\mu\tau - j\omega_c\tau\right)$$

where

$$Q = \frac{1}{2} \frac{\sin\theta_s \sin(\theta_t - \theta_s)}{M \tan\alpha_s \sin\theta_t [b^2 + 4(1+b)\sin^2(\theta_s/2)]}$$

$$B = \sqrt{2}\, kv \tan\beta_o \left[\left(s \frac{\sin\eta_s}{\tan\alpha_s} \sin\phi_v \right)^2 + \left(\frac{N}{2M} \cos\phi_v \right)^2 \right]^{1/2}$$

$$\mu = kv \cos\phi_v \sin\eta_s$$

$$k = 2\pi/\lambda$$

The power spectral density, $\Phi_e(\omega)$, is the Fourier Transform of the autocorrelation function. $R_e(\tau)$ is easily transformed to give

$$\Phi_e(\omega) \cong P_d Q B^{-1} \sqrt{2\pi} \exp\left[-\frac{1}{2B} (\omega - \omega_c + \mu)^2 \right]$$

The shape of the power spectral density will be recognized as being Gaussian. the significance of the parameters Q, B, and μ is now clear. The total reflected power received is $P_d Q$, which is seen by integrating the power spectral density. The parameter B is the value of $\omega - \omega_c + \mu$ at which Φ_e falls to e^{-1} times its maximum value. The "3-dB bandwidth" of Φ_e, or the distance between the points where it has one-half its maximum value, is 0.441 B Hz. The parameter μ is the offset of the peak of the power spectral density from the carrier frequency ω_c.

3.3 REFLECTION COEFFICIENT CONSIDERATIONS

The model used thus far has assumed that the surface was perfectly conducting. According to Beckmann and Spizzochino (1963), when the reflecting surface is not perfectly conducting, we may simply multiply the perfect-conductor reflected wave by the Fresnel reflection coefficient for the surface, as if the surface were smooth and flat. This is an approximation,

since the reflection coefficient is a function of the local incidence angle and this angle varies from place to place on the rough surface. However, the approximation is good when the mean slope of the surface (β_0) is small, as we have assumed in our case.

The reflection coefficient of a surface depends on whether the wave is vertically or horizontally polarized with respect to the surface. A vertically polarized wave has its electric vector in the plane formed by the incident and reflected rays. The reflection coefficient is, in general, complex, because reflection introduces a phase shift as well as an amplitude reduction. For any surface the reflection coefficient for <u>vertically</u> polarized waves is given by

$$R_v = \frac{n^2 \sin\theta - (n^2 - \sin^2\theta)^{1/2}}{n^2 \sin\theta + (n^2 - \sin^2\theta)^{1/2}}$$

and the reflection coefficient for <u>horizontally</u> polarized waves is

$$R_H = \frac{\sin\theta - (n^2 - \cos^2\theta)^{1/2}}{\sin\theta + (n^2 - \cos^2\theta)^{1/2}}$$

where n is the index of refraction of the material and θ is the incidence angle, measured from the horizontal.

The index of refraction for any material is given by

$$n^2 = \epsilon_r + j\ 18\ \sigma/f$$

where ϵ_r = relative permittivity
σ = conductivity
f = frequency, in GHz

For seawater,

$\epsilon_r = 81$
$\sigma = 5$

For pure vertical or horizontal polarization, the fraction of the incident power reflected from a surface is the square of the magnitude of the reflection coefficient, $|R_V|^2$ or $|R_H|^2$. For waves that contain both vertical and horizontal components, the power reflected is the sum of the powers of the vertical and horizontal polarized components, calculated separately. Circular polarized waves have half their power in each linear polarization, so the power reflection coefficient for circular polarized waves is

$$|R_c|^2 = \frac{1}{2}\left[|R_v|^2 + |R_H|^2\right]$$

3.4 ANTENNA POLARIZATION MISMATCH CONSIDERATIONS

A receiving antenna is designed to receive signals with a particular polarization, and its gain is a maximum for waves having that polarization. When received waves have a polarization other than that for which the antenna was designed, the antenna absorbs that fraction of the incident wave that is polarized properly, and rejects the fraction that is orthogonally polarized. The fraction of power of an arbitrarily polarized wave that an antenna will absorb, compared to what it would absorb if the wave were polarized to match the antenna, is given by the polarization mismatch factor, m_p. When the antenna is purely circular polarized, the mismatch factor becomes the following

$$m_p = \frac{1}{2} \pm \frac{r}{r^2+1}$$

where r is the axial ratio of the wave. The axial ratio is the maximum magnitude of the electric field vector divided by its minimum value. The sign in the above equation is positive when the polarization sense (right-hand/left-hand) of the wave and the antenna are the same, and is negative otherwise.

When a pure circularly polarized wave is reflected from a water surface, the axial ratio of the wave becomes

$$r = |R_H|/|R_v|$$

Furthermore, the sense of wave is reversed upon reflection, so if the transmitted wave polarization was right-hand circular, for example, the reflected wave would be mostly left-hand circular polarized. An antenna designed to receive the right-hand circular direct signal would therefore tend to reject the left-hand component of the reflected signal. This rejection of the reflected signal is total when the receiver is directly above the transmitter, because in that case the reflected wave is purely circular polarized. When the incidence angle is less than 90^0, the reflected wave is elliptically polarized (it has an axial ratio greater than one) so the antenna accepts some of the reflected power. In the worst case, at very small incidence angles the reflected wave is nearly linearly polarized (axial ratio very large), and the antenna rejects only half the reflected power.

3.5 BANDPASS FILTERING CONSIDERATIONS

We assume a narrow bandpass filter is used in the receiver to reduce thermal noise and multipath interference. The filter is tuned to the direct signal via a tracking loop. In general, the multipath signal's Gaussian-shaped spectrum is centered about a frequency that is removed from the direct signal, due to the difference in range rate between the platform and the spectral reflecting point. Thus only a fraction of the total reflected signal power will be seen after filtering. That fraction is given by

$$F = \frac{1}{\sqrt{2\pi}\,B} \int_{\omega_c+\omega_d-\frac{\Delta}{2}}^{\omega_c+\omega_d+\frac{\Delta}{2}} \exp\left[-\frac{(\omega-\omega_c+\mu)^2}{2B^2}\right] d\omega$$

where Δ is the filter bandwidth in rad/sec and ω_d is the direct signal Doppler.

3.6 SUMMARY

Combining all the above factors, the following expression is obtained for the ratio of reflected power to direct power received at the satellite:

$$\overline{\rho^2} = |R_c|^2 m_p Q F$$

IV. NUMERICAL RESULTS AND OBSERVATIONS

The analytical results of section II and III were applied to the location system described in section I (Table 1.1). The various formulas were incorporated into a computer program that determined the required geometric variables at regularly spaced points during the satellite overpass. Computations were performed for a number of overpasses at varying closest approach distances from the balloon transmitter. This yieled rms phase and frequency measurement errors for an array of points in the vicinity of the transmitter. The error values associated with each point represented the multipath contribution to the errors as the spacecraft passed through that point. By interpolating between the values obtained for the array, the phase and frequency error contours shown in Figures 4.1 and 4.2 were produced.

The coordinates of the figures are distances from the transmitter in the directions parallel and perpendicular to the satellite subtrack, measured in terms of the Earth central angle. These central angles would represent longitude and latitude if the transmitter were on the equator and the satellite subtrack were directed north-south. The contours plotted in Figure 4.1 are lines of constant rms phase measurement error, expressed in units of dBradians, or ten times the (base 10) logarithm of the error in radians. For reference, 1^{o} = -17.6 dBradian. The contours of Figure 4.2 are in units of dBHz, or ten times the logarithm of the rms frequency error in Hertz.

We note that the maximum values of the multipath errors occuring within the 10^{o} elevation angle circle (2.7^{o} and 0.09 Hz) may be

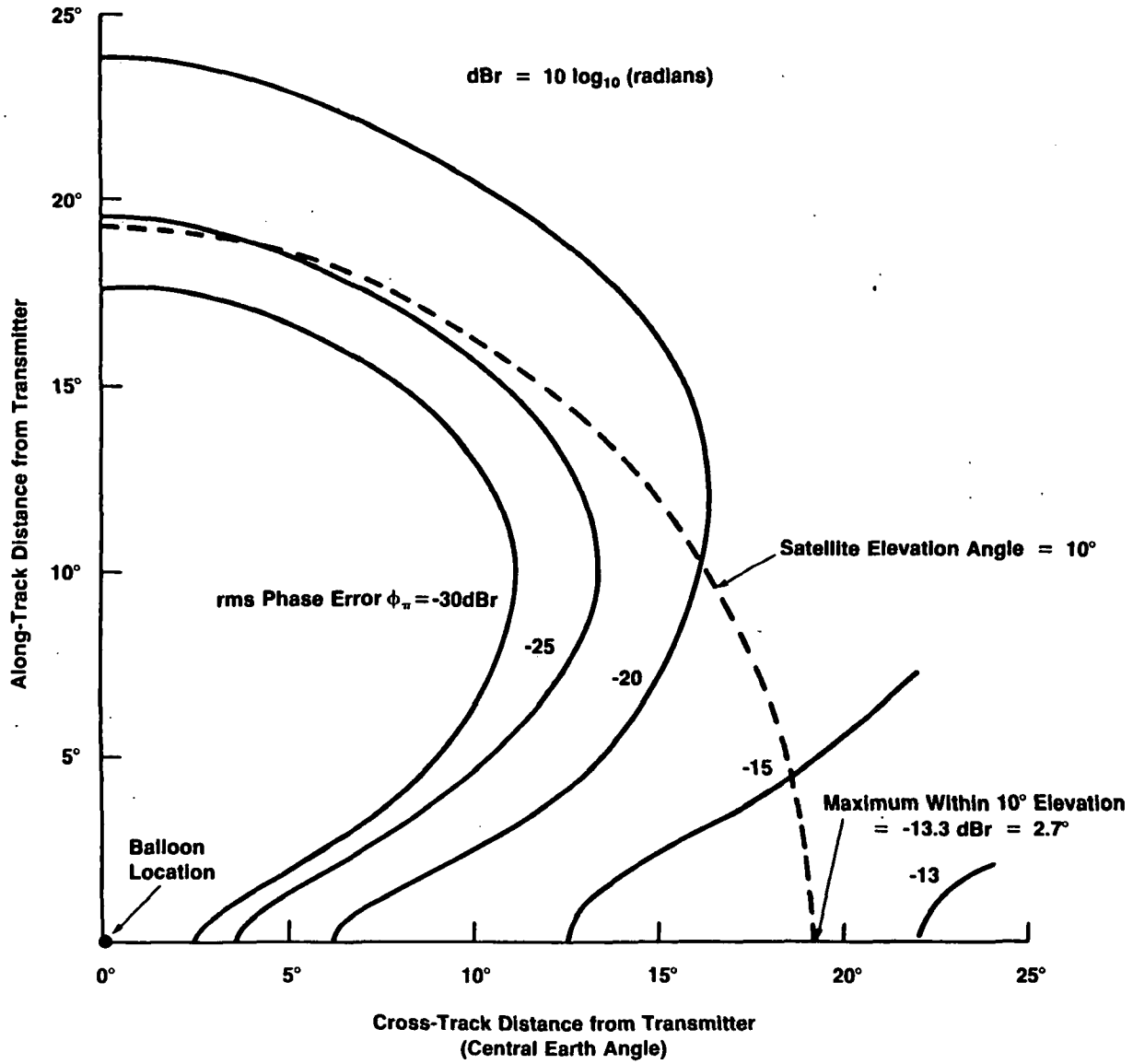

FIGURE 4.1. PHASE ERROR CONTOURS

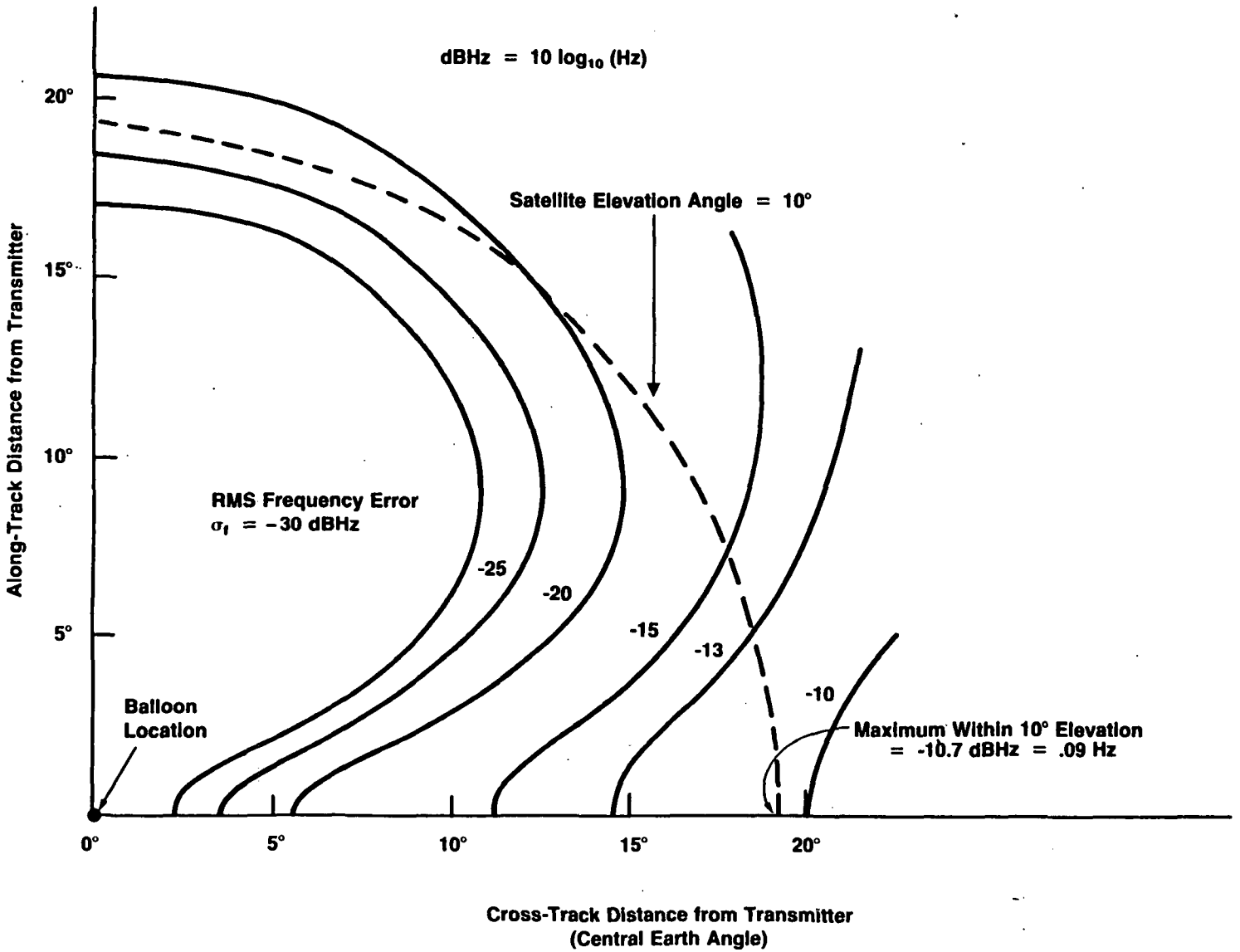

FIGURE 4.2. FREQUENCY ERROR CONTOURS

comparable to errors induced by thermal noise. However, the errors are much less than the maxima over most of the area. We further note that the contours for phase error and frequency error are very similar in shape. This is to be expected, because the only difference in their functional dependencies is a factor of sin (x/2) (see section 2.1), which does not vary greatly over the plane. The shapes of the contours can generally be explained as follows: (1) the errors increase with the distance from the transmitter, in large part due to the increase in the antenna polarization mismatch factor, m_p. (2) the error goes through a peak value at the point of closest approach. This is caused by the peak of the multipath signal spectrum passing through the bandpass filter. The frequency difference between the direct signal (where the measurement filter is centered) and the peak of the multipath signal is determined by the range rate difference between the transmitter and the spectral reflection point. But at closest approach, both points are abeam of the spacecraft, and their range rates are both zero. When this happens, the multipath signal is centered in the filter passband.

Figure 4.3 shows the rms multipath location error from multipath if a location determination were made using the interferometer on the basis of a single transmission received at the point of closest approach. This corresponds to the worst case for multipath-induced error. For comparison, the rms location error induced by thermal noise is also shown in the figure. The rms phase variance due to thermal noise was assumed to be 0.02 radians, or 1.15 degrees. Multipath-induced error is roughly twice the thermal noise-induced error for this case. Note that the error shown here is highly atypical corresponding to a transmission received exactly at closest approach. Location error will be reduced in a real system by using measurements from all the transmissions received during the overpass.

The curves presented here do not take into account antenna patterns. It assumes that the antennas are isotropic and perfectly circular polarized. If the antenna used by the balloon trasmitter had a radiation pattern designed to reduce multipath, the error contours could be altered drastically. The ideal antenna for this purpose would have no radiation below the horizon and an isotropic pattern above the horizon. This is not possible to achieve, and

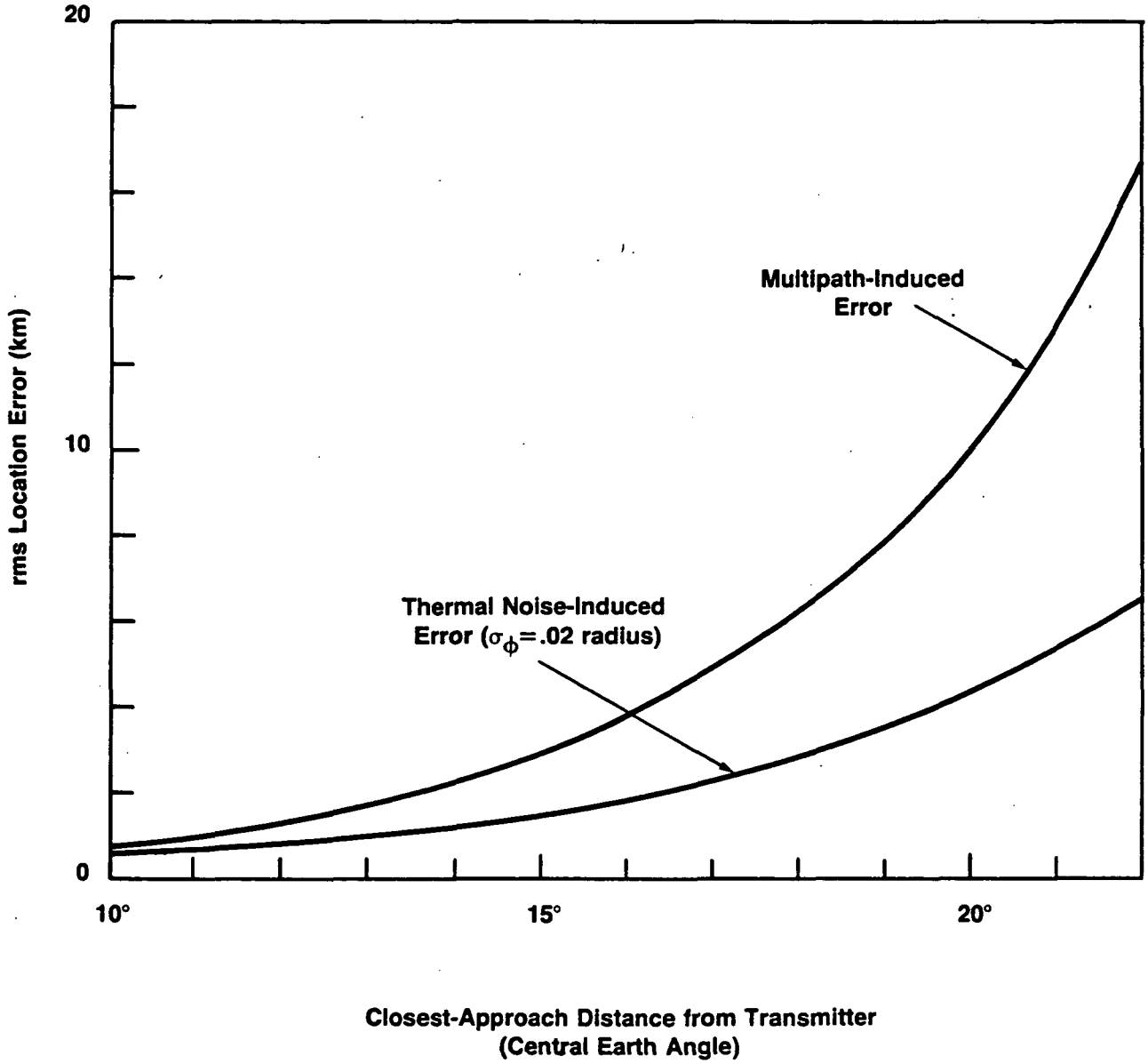

FIGURE 4.3. WORST-CASE LOCATION ERROR FOR SINGLE-TRANSMISSION LOCATION

the closeness with which it may be approached is limited in the case of meteorological balloons by the requirements for low cost, lightness, and frangibility. The error contours with a practical transmitter antenna must be modified by subtracting from the error, in dBradians or dBHz, the quantity

$$1/2\ [G(90^{o}+e) - G(90^{o}-e)]$$

where G is the antenna power gain in dBi (relative to a zenith axis) and e is the elevation angle of the satellite. Assuming the antenna was designed to reduce multipath effects, this would have the effect of pushing all the contours away from the origin.

V. REFERENCES

Beckman, P. and A. Spizzichino (1963), The Scattering of Electromagnetic Waves from Rough Surfaces, Pergamon Press, Oxford.

Blanchard, Alain (1976), Phase-Locked Loops, John Wiley and Sons, N.Y., p. 355.

Duncan, J.W. (1967), "The Effects of Ground Reflections and Scattering on an Interferometer Direction Finder," IEEE Trans. Aerospace and Elect. Systems, Vol. AES-3, No. 6, November 1967, pp. 922-932.

Duranni, S.H., and H. Staras (1968), "Multipath Problems in Communications Between Low-Altitude Spacecraft and Stationary Satellites," RCA Review, March 1968, pp. 77-105.

Reed, D.L. and R. G. Wallace, (1981), "NOSS/ALDCS Analysis and System Requirements Definition," ORI Technical Repot 1864, February 1981. Prepared for NASA/GSFC under contract NAS5-26164.

Staras, H. (1968), "Rough Surface Scattering on a Communications Link," Radio Science, Vol. 3, No. 6, June 1968, pp. 623-631.

Muehldorf, E.I. (1971), "The Effect of Multipat Reflections in Spaceborne Interferometer Accuracy," IEEE Trans. Aerosp. and Elect. Systems, Vol. AES-7, No. 1, January 1971, pp. 122-131.

Wallace, R.G., and D.L. Reed (1981), "Analysis of Meteorological Location and Data Collection System Concepts," ORI Technical Report 1989, December 1981. Prepared for NASA/GSFC under contract NAS5-26604.

APPENDIX
DERIVATION OF TAYLOR SERIES EXPANSIONS

The method of steepest descent for evaluating integrals containing exponentials depends on writing an approximation for the exponent that holds in the vicinity of a stationary point. At a stationary point, a function takes on an extreme value (maximum or minimum). It is therefore the point where its first derivatives vanish. In our case the function is $\tan^2$ (the real part of the exponent), which is a function of and . The stationary point turns out to be the point of specular reflection, where = $_s$ and = 0. The approximation made for $\tan^2$ at the stationary point contains only the quadratic terms in and , since $\tan^2$ vanishes at that point. the approximation is

$$\tan^2\beta \cong \frac{\partial^2}{\partial\theta^2}\left(\tan^2\beta\right)\Big|_{\substack{\theta=\theta_s\\ \phi=0}}(\theta-\theta_s)^2 + \frac{1}{2}\frac{\partial^2}{\partial\phi^2}\left(\tan^2\beta\right)\Big|_{\substack{\theta=\theta_s\\ \phi=0}}\phi^2$$

From Staras (1968), we have $\tan^2$ in terms of the angles $_1$, $_2$ and p (the angle between the surface projections of the incident and reflected rays):

$$\tan^2\beta = \frac{\sin^2\alpha_1 + \sin^2\alpha_2 - 2\sin\alpha_1\sin\alpha_2\cos\rho}{(\cos\alpha_1 + \cos\alpha_2)^2}$$

The angle p can be related to ϕ as follows by applying some spherical trigonometry and making the approximation $\cos\phi \cong 1$. (This will prove to be a good approximation for surface points in the vicinity of the specular reflection point.)

$$\cos \rho = \left[1 - \frac{\sin^2\theta_t \sin^2\phi}{\sin^2(\theta_t-\theta)}\right]^{1/2}$$

Using this, it turns out after tedious calculation

$$\left.\frac{\partial^2}{\partial\phi^2}(\tan^2\beta)\right|_{\substack{\theta=\theta_s \\ \phi=0}} = \frac{1}{2}\tan^2\alpha_s \frac{\sin^2\theta_t}{\sin^2(\theta_t-\theta_s)}$$

$$\left.\frac{\partial^2}{\partial\theta^2}(\tan^2\beta)\right|_{\substack{\theta=\theta_s \\ \phi=0}} = \frac{1}{2}\left(\frac{\partial\alpha_1}{\partial\theta} - \frac{\partial\alpha_2}{\partial\theta}\right)^2\Bigg|_{\substack{\theta=\theta_s \\ \phi=0}}$$

$$= \frac{1}{2}\left[(1+b)\frac{1+b-\cos(\theta_t-\theta_s)}{(1+b)^2-2(1+b)\cos(\theta_t-\theta_s)} + (1+c)\frac{1+c-\cos\theta_s}{(1+c)^2-2(1+c)\cos\theta_s}\right] = 2M^2$$

with $b = h_1/a$ and $c = h_2/a$. The first term of this may be rewritten for improved precision with small $(\theta_t-\theta_s)$ by using

$$\cos x = 1 - 2\sin^2(x/2)$$

The imaginary part of the exponent,

$$I = \cos(\phi_v + \phi)\sin\eta$$

is approximated by a constant and a linear term in both θ and ϕ.

$$I \cong I\Big|_{\substack{\theta=\theta_s \\ \phi=0}} + \frac{\partial I}{\partial \theta}\Big|_{\substack{\theta=\theta_s \\ \phi=0}} (\theta-\theta_s) + \frac{\partial I}{\partial \phi}\Big|_{\substack{\theta=\theta_s \\ \phi=0}} \phi$$

$$I\Big|_{\substack{\theta=\theta_s \\ \phi=0}} = \cos\phi_v \sin(\alpha_s-\theta_s)$$

$$\frac{\partial I}{\partial \phi}\Big|_{\substack{\theta=\theta_s \\ \phi=0}} \cong -\sin\phi_v \sin\eta_s$$

$$\frac{\partial I}{\partial \theta}\Big|_{\substack{\theta=\theta_s \\ \phi=0}} \cong N\cos\phi_v = \frac{(1+c)\cos\theta_s - 1}{(1+c-\cos\theta_s)^2}\left[1+\left(\frac{\sin\theta_s}{1+c-\cos\theta_s}\right)^2\right]^{-3/2} \cdot \cos\phi_v$$